ResearchGate

See discussions, stats, and author profiles for this publication at: https://www.researchgate.net/publication/344069973

SYNTHESIS AND STRUCTURE DETERMINATION OF NOVEL MIXED VALENCE Pb 0.5 U0.25 Zr 1.25 O4.5 BY POWDER XRD OBTAINED FROM PbCO3 -U(CO3)2 -Zr(CO3)2 TERNARY MIXED VALENCE OXIDES

Article · September 2020

CITATION
1

READS
4

2 authors, including:

Parashuram Mishra
Tribhuvan University
215 PUBLICATIONS **2,183** CITATIONS

SEE PROFILE

Some of the authors of this publication are also working on these related projects:

Oxidation of Penicillanic acid derivatives / Techniques of degradation of antibiotics View project

Crystal Growth and Design structure determination View project

All content following this page was uploaded by Parashuram Mishra on 03 September 2020.

The user has requested enhancement of the downloaded file.

SYNTHESIS AND STRUCTURE DETERMINATION OF NOVEL MIXED VALENCE

$Pb_{0.5}U_{0.25}Zr_{1.25}O_{4.5}$ BY POWDER XRD OBTAINED FROM $PbCO_3$ -$U(CO_3)_2$ -$Zr(CO_3)_2$ TERNARY MIXED VALENCE OXIDES

Bimal K.Kanth and Parashuram Mishra*,Bioinorganic and Material Chemistry Research Lab.Tribhuvan University,M.M.A.M.Campus,Biratnagar, Nepal

Abstract

A novel mixed valence metal oxide , namely **$Pb_{0.5}U_{0.25}Zr_{1.25}O_{4.5}$**, has been successfully synthesized by high-temperature solid-state reaction in open air atmosphere for the first time. X-ray powder diffraction coupled with Rietveld refinement reveals the sample's phase purity we have prepared. Thermal behavior analysis shows **$Pb_{0.5}U_{0.25}Zr_{1.25}O_{4.5}$** is very stable, it doesn't decomposition until heated up to 998 °C. UV-visible absorption and diffuse reflection spectrum feature characteristic absorption bands of *f*-electron transition and an optical bandgap value of 4.65 eV. Magnetic susceptibilities measurement gives significant antiferromagnetic interactions between magnetic centers. The photodegradation experiments were performed to evaluate photocatalytic activities of **$Pb_{0.5}U_{0.25}Zr_{1.25}O_{4.5}$**.**The** Lattice parameters a=1.855 Å, b=1.1937 Å, c=8.8785 Å, α=90.1230° β=94.2069° γ=91.2743. ° and V=134.48 $Å^3$. Chemical analysis of several crystallites by EDX is in agreement with the formula **$Pb_{0.5}U_{0.25}Zr_{1.25}O_{4.5}$**, Moreover, the structure was independently determined by Rietveld refinement from X-ray powder data obtained from a multi-phasic sample. The morphology of the crystal was carried out by AFM,TEM and SEM.

Key-words:- Powder XRD,SEM,TEM,lattce parameter,Rietveld refinement

INTRODUCTION

Mixed valence metal oxides continue to be the subject of intensive research due to their potential uses as prospective materials for different applications related to their specific properties such as ionic conductivity, piezoelectricity, luminescence, catalysis and magnetism [1]. Iron phosphates are of particular interest because they offer a variety of structural types in which Zr adopts the oxidation states +4 and forms with oxygen atoms various coordination The interest in of **$Pb_{0.5}U_{0.25}Zr_{1.25}O_{4.5}$**.. Materials with pronounced twinning or new compounds that only exist as part of a complex multi-phase powder sample are thus extremely difficult to treat with this standard method for structure determination. It should be noted that these problem cases also include many technologically relevant products such as small precipitates in a metallic matrix, catalysts, pharmaceuticals, pigments and thin films, which a priori exist only in small quantities or rarely grow as large crystals. Hence, ample motivation exists to develop alternative approaches capable for structural analysis of extremely small volumes and crystallites. However, the only real alternative to X-rays is fast electrons, since their interaction with matter is several orders of magnitude stronger than that of X-rays. Electron diffraction structure analysis (EDSA) makes it,

thus, possible to obtain structural information at the atomic level even for the steadily growing number of nanocrystalline materials[2]. On the other hand, structure analysis with electron data is rarely straight forward and fully automated, as it is the case with X-ray data. In particular, the non-kinematical nature of the diffracted intensities is a great concern for structure analysis with electron diffraction data and has hindered EDSA from becoming very popular since its foundation in Russia more than 65 years ago. While a large number of light-atom structures have been investigated by electron diffraction in the past [3], it has only succeeded in a few cases to In the last few years intensive research work has been undertaken on a new bismuth-based mixed oxide family, showing a characteristic columnar [PbO-ZrO_2 -UO_2] arrangement, because of its potentially good ionic conductivity properties. The high-temperature polymorph of the compound **Pb $_{0.5}$ U$_{0.25}$ Zr $_{1.25}$ O$_{4.5}$ .T**he phase oxide belonging to this columnar structural type to be described. Its structure was solved by X –ray powder diffraction solve structures with heavier atoms directly from electron diffraction patterns . In order to avoid these problems, an alternative approach was developed for such non-light-atom structures[4]. This approach exploits the low-order structure factor phases extracted from high-resolution electron microscopy. In this context, we have chosen to explore the ternary diagram PbO-ZrO2 UO2. A new compound was identified from the powder X-ray diffraction (XRD) pattern of one of the synthesized samples. According to its position in the phase diagram, this new phase was supposed to be **Pb $_{0.5}$ U$_{0.25}$ Zr $_{1.25}$ O$_{4.5}$.** Experimentally, the chance to get polycrystalline materials is generally larger than to get single crystals. In this case, powder X-ray diffraction (PXRD) becomes a popular technique but with this technique, the possibility to determine an unknown structure dramatically decreases, because 3D reflections are compressed into 1D with an inevitable overlapping problem, especially when the unit cell is big. The situation will become worse when the PXRD is collected on a multi-phase sample, which is not uncommon in the preliminary stage of searching new materials[5] .The difficulty could further increase when the target phase is not the highly dominant one in the composition. To determine the structure of an unknown phase in a multi-phase polycrystalline sample would be very helpful for the researchers, saving time to optimize the syntheses condition Several mature analysis methods, such as the direct method,1 Patterson method,2 charge-flipping algorithm3 and maximum entropy method4 can be applied to accurately solve the structure and study the electrical properties as well. This paper describes their synthesis and structural study by synthesis and structure determination by powder XRD. Their purities were confirmed by their X-ray powder diagrams collected in the range $10° \leq 2\theta \leq 90°$ on a PANalytical diffractometer using CuKα radiation (λ = 1.5406 Å).

MATERIALS AND METHODS

Reagents: All of the chemical reagents were analytical grade. PbO2 (99.9%), ZrO2 (99.9%), andUO2(99.9%) were used as starting materials as purchased from Sigma Aldrich with no further purification. The mixture was ground carefully, homogenized thoroughly with methanol (99%) in an agate mortar and then packed into an alumina crucible and calcined at 1000°C in air for 10h with several intermediate grindings[6]. Finally the product was pressed into pallets and sintered at 100 K/h. Powder X-ray diffraction (XRD) data were collected at room temperature in the angular range of2θ =10 to 90 with scan step width of 0.02° and a fixed containing time of 15 s using Philips powder diffractometer with graphite monochromatic CuKa radiation. The powder was rotated during the data collection to minimize preferred Orientation effect if any. The program TREOR in CRYSFIRE was used to index the powder pattern which give orthorhombic cell system.SIRPOW92 was used to locate the positional parameters of constituent

atoms. The full pattern is fitting and peak decomposition in the space group Pcnb using check cell program. The structural parameters were refined by the Reitveld method using the GSAS program which gave Rwp = 0.0317, Rp= 0.022, Rp = 0.052. The density is determined by Archimedes principle. The morphology of titled compound was determined using AFM (Nanoscope III, Digital Instruments, Santa Barbara) For the electrical studies, the measurements were preceded by a pretreatment of the sample in order to reduce the mean particle size of the obtained powder After these treatments, the sample achieved about 85% of the theoretical density with the final diameter of 8 mm and thickness of 2 mm. The relative density of the sample before the mechanical grinding was 79 %. Platinum electrodes were connected to the two faces of thepellet via a platinum paste to keep good electric contacts. Impedance spectroscopy measurements were carried out using a Hewlett-Packard 4192a Impedance Analyzer. The impedance spectra were recorded in the 5 Hz-13 MHz frequency range. Electrical conductivity measurements of representative $\mathbf{Pb_{0.5}U_{0.25}Zr_{1.25}O_{4.5}}$ were carried out by complex impedance spectroscopy with a 1174 Solartron frequency response analyzer coupled to a 1286 Solartron electrochemical interface. Pellets of about 14 mm diameter and 1 mm thickness were prepared by cold pressing of a mechanically activated powder mixture with the composition: $\mathbf{Pb_{0.5}U_{0.25}Zr_{1.25}O_{4.5}}$.To form the phase, the pellets were heated at 7003C during 12 h and slowly cooled to room temperature. This synthesis method was employed to improve the ceramic quality, as it has been shown for other materials [7]. The formed phases and crystallinity were studied by X-ray powder diffraction. Platinum electrodes were deposited on the two faces by sputtering, and measurements were carried out in the temperature range 200}6503C, at steady temperatures, with pellets under air flow. The frequency range was fixed.

RESULTS AND DISCUSSION

In materials chemistry, the crystal structure determination is the first step to understand and interpret physical properties of an unknown material. Moreover, it also guides people on how to modify the material and hence improve the performance[8]. Nowadays, the most successful technique for structure determination is through single crystal X-ray diffraction, from which a sufficient number of independent reflections against the structural parameters can be extracted in 3D reciprocal space. Several mature analysis methods, such as the direct method,1 Patterson method,2 charge-flipping algorithm3 and maximum entropy method4 can be applied to accurately solve the structure. This technique requires synthesizing a high quality single crystal at a micrometer. Experimentally, the chance to get polycrystalline materials is generally larger than to get single crystals. In this case, powder X-ray diffraction (PXRD) becomes a popular technique but with this technique, the possibility to determine an unknown structure dramatically decreases, because 3D reflections are compressed into 1D with an inevitable overlapping problem, especially when the unit cell is big. The situation will become worse when the PXRD is collected on a multi-phase sample, which is not uncommon in the preliminary stage of searching new materials, especially in the cases of hydrothermal (or solvothermal) syntheses of zeolitic or MOF materials'XRD data for the sample of $\mathbf{Pb_{0.5}U_{0.25}Zr_{1.25}O_{4.5}}$synthesized at its nominal composition is shown in Figure 1. All peaks could be indexed to a triclinic unit cell with *P-1* symmetry, analogous to the $\mathbf{Pb_{0.5}U_{0.25}Zr_{1.25}O_{4.5}}$structure using CRYSFIRE PACKAGE11]. In the diffraction pattern there is a slight anisotropic peak broadening moving to higher angles. This slight peak broadening could be caused by ordering within the cationic layers but relative disorder of the cations between layers. The sloping background observed in XRD at low angles

out to ~30° 2θ is qualitatively indicative of stacking faults, a common feature of honeycomb oxides. In an ideal layered mixed-metal oxide, all the cationic planes are stacked along the c-axis by a unique translational stacking vector. However it has been shown that two other stacking vectors with very similar energy (1-2 meV) can occur in a structure, leading to so called "stacking faults". Stacking faults in the honeycomb oxides occur due to the relatively weak coupling between the layers In practice, the cationic layers are never perfectly stacked along the c-axis when a layered structure has the *P*-1space group, although higher temperature thermal treatment during synthesis can decrease the frequency of stacking faults[12].

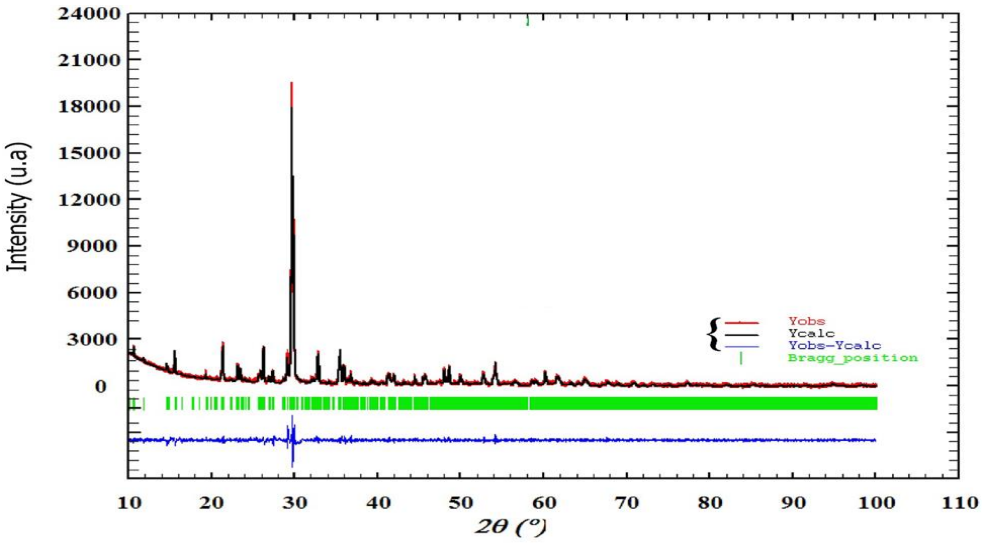

Figure1 Rietveld refinement of powder **Pb** $_{0.5}$ **U**$_{0.25}$ **Zr** $_{1.25}$ **O**$_{4.5}$

Rietveld refinement of Triclinic with P1 space group **Pb** $_{0.5}$ **U**$_{0.25}$ **Zr** $_{1.25}$ **O**$_{4.5}$against XRD data for structural determination proved difficult, due to a combination of preferred orientation of the plate-like crystallites in flat-plate geometry[9].In other words, the extracted peak intensities for phase 1 could be reliable. Note that if the relative intensities differed a lot from the simulated patterns of the known phases, additional manual partitioning of those overlapping peaks would be necessary to get reliable intensities for the unknown phase 1. After considering themultiplicity and Lorentz-polarization correction, the intensities of phase 1 were used for the structure solution as below. Moreover, the reflection conditions indicated possible space groups Pcnb . The initial structure model was obtained using a charge flipping algorithm with the program Superflip.8 [13]Random phases were used at the beginning of the charge-flipping iteration, and overlapping peaks were re-partitioned using a histogram match to improve the convergence. The iteration converged with an R factor of 29% and the final electron density shows aP-1 symmetry with a 5% error. The program of EDMA was then used to automatically assign atomic positions. Four unique heavy atomic positions were found and the heaviest one was assigned as Zr while the others were considered as Zr and U.Due to the existence of heavy atoms, all oxygen positions were ambiguous in the electron density map of this stage[14]. To locate the oxygen atoms, a Monte-Carlo based simulated annealing process with the program TOPAS was applied. For each annealing process, various atomic coordinates were randomly assigned as the initial positions of the oxygen atoms [10]. The annealing process was restarted after finding a few oxygen positions, until all oxygen positions were found to be reasonable.

Table1

Crystallography data of Pb $_{0.5}$ U$_{0.25}$ Zr $_{1.25}$ O$_{4.5}$

Formula sum	**Pb $_{0.5}$ U$_{0.25}$ Zr $_{1.25}$ O$_{4.5}$**
Formula weight	552.4 g/mol
Crystal system	triclinic
Space-group	P -1 (2)
Cell parameters	a=1.855(11) Å b=8.1937 Å c=8.8785 Å α=94.2069° β=91.2574° γ=91.7243°
Cell ratio	a/b=0.2264 b/c=0.9229 c/a=4.7863
Cell volume	134.48(80) Å^3
Z	2
Calc. density	13.6408 g/cm^3
Exp.density	12.163g/cm^3
Pearson code	aP22
Formula type	N2O3P4Q13
Wyckoff sequence	i10gb

Table 2Atomic coordinate

Atomic parameters								
Atom	**Ox.**	**Wyck.**	**Site**	**S.O.F.**	**x/a**	**y/b**	**z/c**	**U [Å^2]**
U1		2i	1		0.38413	0.22326	0.24012	0.0380
Pb1		1b	-1		0	0	1/2	0.0380
Pb2		2i	1		-0.29667	-0.33621	0.16712	0.0380
Zr1		2i	1		0.12846	-0.04514	0.07499	0.0380
Zr2		2i	1		-0.22113	-0.09420	0.35433	0.0380
Zr3		1g	-1		-1.00000	-1/2	1/2	0.0380
Zr4		2i	1		-0.54078	-0.26947	0.33187	0.0380
Zr5		2i	1		0.77556	0.48579	0.07293	0.0380
Zr6		2i	1		0.11202	-0.23568	0.04884	0.0380
Zr7		2i	1		0.43390	0.42272	-0.00054	0.0380
O1		2i	1		0.26714	-0.32853	0.06861	0.0380
O2		2i	1		-0.60400	-0.33634	0.48128	0.0380

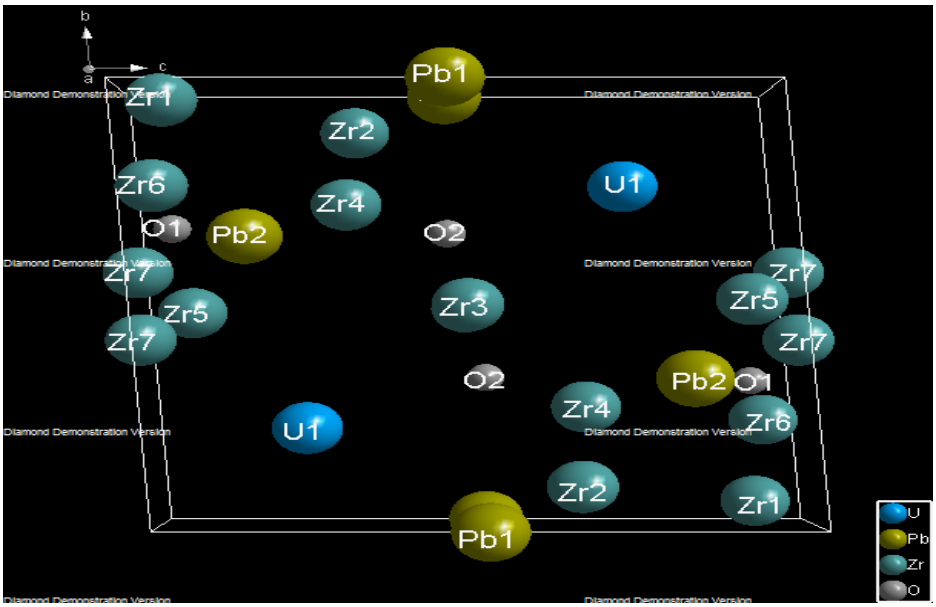

Figure 2. Representation of the powellite-type crystal structures of **Pb $_{0.5}$ U$_{0.25}$ Zr $_{1.25}$ O$_{4.5}$**.atoms

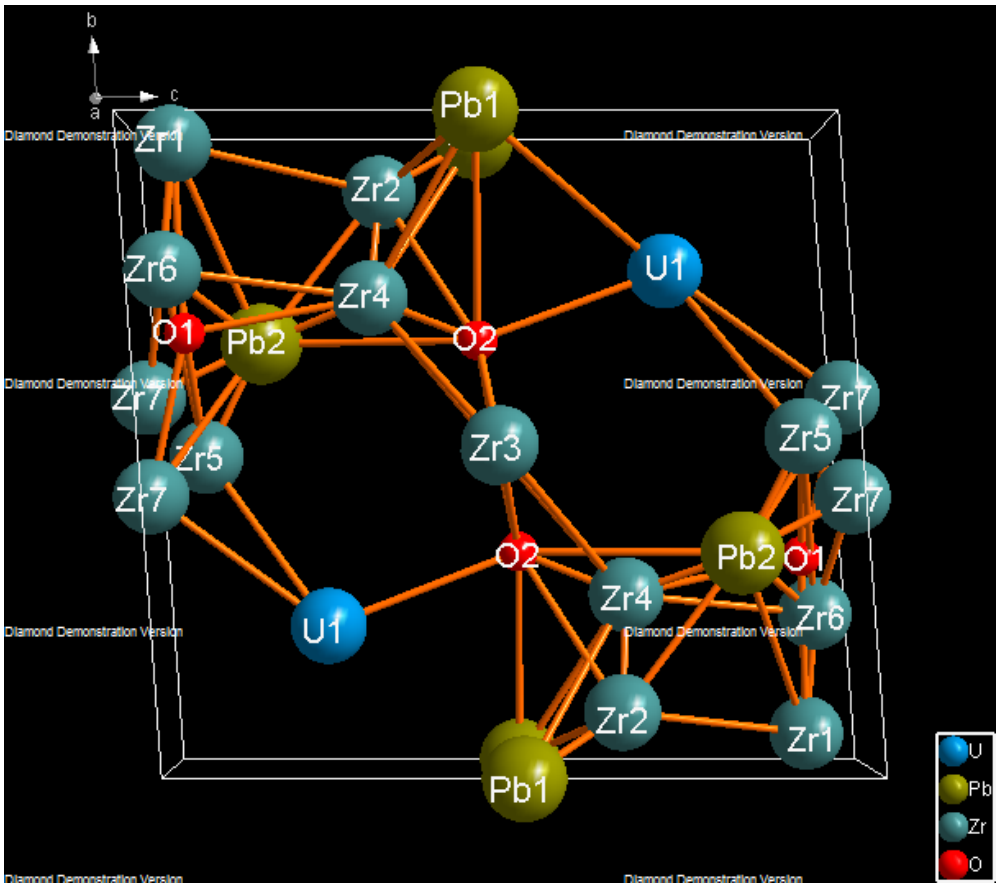

Figure.3 3D structure Structure model of $Pb_{0.5}U_{0.25}Zr_{1.25}O_{4.5}$ in projection along the short c-axis as obtained from Rietveld refinement

Table.3 Bond angles

Atom1	Atom code	Atom2	Atom code	Angles
O1	11455011	Zr4	7555011	115.5325
Zr6	9555011	Zr4	7555011	126.760
Zr6	9555011	Zr7	10555021	70.285
Zr6	9555011	Zr5	8445011	95.261
Zr6	9555011	Zr6	9455011	67.196
Zr6	9555011	Pb2	3655011	61.298
Zr6	9555011	Pb2	3455011	118.702
Zr6	9555011	Zr4	7655011	91.929
Zr6	9555011	Zr7	10655021	51.404
Zr6	9555011	Zr5	8345011	116.627
Pb2	3655011	Pb2	3455011	180.000
Pb2	3655011	Zr4	7655011	48.366
Pb2	3655011	Zr7	10655021	43.894

	Pb2	3655011	Zr5	8345011	135.5722
Zr1	Zr6	9555011	Zr1	4555021	112.920
	Zr6	9555011	Zr1	4655011	89.208
	Zr6	9555011	Zr1	4455011	90.792
	Zr6	9555011	Zr1	4655021	107.011
	Zr6	9555011	O1	11555011	10.170
	Zr1	4555021	O1	11555011	121.790
	Zr1	4655011	O1	11555011	81.935
	Zr1	4455011	O1	11555011	98.065
	Zr1	4455011	Zr6	9455011	40.403
	Zr1	4455011	Zr6	9655011	140.253
	Zr1	4655021	O1	11555011	106.740
	Zr1	4655021	Zr6	9455011	134.379
	Zr1	4655021	Zr6	9655011	71.592
	O1	11555011	Zr6	9455011	57.998
	O1	11555011	Zr6	9655011	42.605
	Zr6	9455011	Zr6	9655011	99.850
Zr2	Pb1	2555011	Zr4	7555011	127.855
	Pb1	2555011	Zr2	5455011	103.837
	Pb1	2555011	O2	12555011	92.963
	Pb1	2555011	Pb2	3555011	155.897
	Zr4	7555011	Pb2	3555011	38.429
	Pb1	2455011	O2	12555011	77.992
	Pb1	2455011	Pb2	3555011	129.780
	O2	12555011	Pb2	3555011	70.755
Zr3	O2	12346021	O2	12555011	180.000
	O2	12346021	O2	12446021	67.449
	O2	12346021	O2	12455011	112.551
	O2	12346021	Zr3	6655011	117.116
	O2	12346021	Zr3	6455011	62.884
	O2	12555011	O2	12446021	112.551
	O2	12555011	O2	12455011	67.449
	O2	12555011	Zr3	6655011	62.884
	Pb2	3555011	Zr4	7455011	108.224
	Pb2	3555011	Zr4	7655011	71.776
	Pb2	3555011	Zr2	5455011	120.262
	Pb2	3555011	Pb2	3455011	59.858
	Pb2	3555011	O2	12655011	102.401
	Pb2	3555011	O1	11455011	26.828
	Pb2	3555011	O2	12455011	131.805
	Pb2	3665011	Zr6	9665011	41.348
	Pb2	3665011	Zr7	10565021	75.413
	Zr5	8665021	O1	11655021	64.597
	Zr5	8665021	O1	11665011	96.241
	Zr5	8665021	Zr7	10765021	97.165
	Zr5	8665021	O1	11565011	59.435

Zr5	8665021	Zr5	8455011	53.082
Zr5	8665021	Zr5	8655011	126.918
Zr5	8665021	Zr6	9655021	83.142
Zr5	8665021	Pb2	3765011	126.053
Zr5	8665021	Zr6	9665011	83.181
Zr5	8665021	Zr7	10565021	35.787
O1	11655021	O1	11665011	125.987
O1	11655021	Zr7	10765021	93.129
O1	11655021	O1	11565011	124.032
O1	11655021	Zr5	8455011	89.574
O1	11655021	Zr5	8655011	90.426
O1	11655021	Zr6	9655021	19.291
O1	11655021	Pb2	3765011	132.830
O1	11655021	Zr6	9665011	127.196
O1	11655021	Zr7	10565021	91.613
O1	11665011	Zr7	10765021	36.726
O1	11665011	O1	11565011	62.588
O1	11665011	Zr5	8455011	119.633
O1	11665011	Zr5	8655011	60.367
O1	11665011	Zr6	9655021	132.931
O1	11665011	Pb2	3765011	29.834
O1	11665011	Zr6	9665011	16.380
O1	11665011	Zr7	10565021	99.472
Zr7	10765021	O1	11565011	93.578
Zr7	10765021	Zr5	8455011	144.955
Zr7	10765021	Zr5	8655011	35.045
Zr7	10765021	Zr6	9655021	96.404
Zr7	10765021	Pb2	3765011	43.577
Zr7	10765021	Zr6	9665011	48.814
Zr7	10765021	Zr7	10565021	120.534
O1	11565011	Zr5	8455011	57.045
O1	11565011	Zr5	8655011	122.955
O1	11565011	Zr6	9655021	142.199
O1	11565011	Pb2	3765011	83.796
O1	11565011	Zr6	9665011	46.749
O1	11565011	Zr7	10565021	39.551
Zr5	8455011	Zr5	8655011	180.000
Zr5	8455011	Zr6	9655021	97.462
Zr5	8455011	Pb2	3765011	135.572
Zr5	8455011	Zr6	9665011	103.648
Zr5	8455011	Zr7	10565021	24.422
Zr5	8655011	Zr6	9655021	82.538
Zr5	8655011	Pb2	3765011	44.428
Zr5	8655011	Zr6	9665011	76.352
Zr5	8655011	Zr7	10565021	155.578

	Zr6	9655021	Pb2	3765011	126.931
	Zr6	9655021	Zr6	9665011	140.183
	Zr6	9655021	Zr7	10565021	105.969
	Pb2	3765011	Zr6	9665011	44.131
	Pb2	3765011	Zr7	10565021	123.339
	Zr6	9665011	Zr7	10565021	83.096
Zr6	O1	11555011	Zr1	4555011	150.920
	O1	11555011	Pb2	3555011	61.049
	O1	11555011	O1	11455011	84.027
	O1	11555011	Pb2	3655011	35.794
	O1	11555011	Zr7	10655021	27.217
	O1	11555011	Zr7	10555021	59.414
	O1	11555011	Zr6	9655011	68.850
	O1	11555011	Zr6	9455011	111.150
	O1	11555011	Zr5	8655021	42.275
	O1	11555011	O1	11655011	48.705
	O1	11555011	Zr5	8445011	35.558
	O1	11555011	Zr1	4655011	106.769
	O1	11555011	Zr1	4455011	146.416
	Zr1	4555011	Pb2	3555011	117.423
	Zr1	4555011	O1	11455011	114.360
	Zr1	4555011	Pb2	3655011	115.181
	Zr1	4555011	Zr7	10655021	150.034
	Zr1	4555011	Zr7	10555021	146.926
	Zr1	4555011	Zr6	9655011	90.792
	Zr1	4555011	Zr6	9455011	89.208
	Zr1	4555011	Zr5	8655021	158.814
	Zr1	4555011	O1	11655011	109.503
	Zr1	4555011	Zr5	8445011	160.089
	Zr1	4555011	Zr1	4655011	50.389
	Zr1	4555011	Zr1	4455011	49.462
	Pb2	3555011	O1	11455011	41.517
	Pb2	3555011	Pb2	3655011	67.196
	Pb2	3555011	Zr7	10655021	85.444
	Pb2	3555011	Zr7	10555021	55.605
	Pb2	3555011	Zr6	9655011	118.702
	Pb2	3555011	Zr6	9455011	61.298
	Pb2	3555011	Zr5	8655021	83.185
	Pb2	3555011	O1	11655011	102.013
	Pb2	3555011	Zr5	8445011	43.391
	Pb2	3555011	Zr1	4655011	131.956
	Pb2	3555011	Zr1	4455011	85.957
	O1	11455011	Pb2	3655011	105.502
	O1	11455011	Zr7	10655021	95.583
	O1	11455011	Zr7	10555021	36.248
	O1	11455011	Zr6	9655011	152.877

O1	11455011	Zr6	9455011	27.123
O1	11455011	Zr5	8655021	77.103
O1	11455011	O1	11655011	132.732
O1	11455011	Zr5	8445011	49.512
O1	11455011	Zr1	4655011	162.384
O1	11455011	Zr1	4455011	65.625
Pb2	3655011	Zr7	10655021	53.476
Pb2	3655011	Zr7	10555021	92.614
Pb2	3655011	Zr6	9655011	51.506
Pb2	3655011	Zr6	9455011	128.494
Pb2	3655011	Zr5	8655021	75.974
Pb2	3655011	O1	11655011	36.779
Pb2	3655011	Zr5	8445011	66.394
Pb2	3655011	Zr1	4655011	78.243
Pb2	3655011	Zr1	4455011	138.173
Zr7	10655021	Zr7	10555021	61.459
Zr7	10655021	Zr6	9655011	60.075
Zr7	10655021	Zr6	9455011	119.925
Zr7	10655021	Zr5	8655021	25.474
Zr7	10655021	O1	11655011	43.091
Zr7	10655021	Zr5	8445011	48.129
Zr7	10655021	Zr1	4655011	100.207
Zr7	10655021	Zr1	4455011	158.929
Zr7	10555021	Zr6	9655011	121.534
Zr7	10555021	Zr6	9455011	58.466
Zr7	10555021	Zr5	8655021	40.870
Zr7	10555021	O1	11655011	103.499
Zr7	10555021	Zr5	8445011	26.420
Zr7	10555021	Zr1	4655011	161.111
Zr7	10555021	Zr1	4455011	97.952
Zr6	9655011	Zr6	9455011	180.000
Zr6	9655011	Zr5	8655021	82.538
Zr6	9655011	O1	11655011	20.145
Zr6	9655011	Zr5	8445011	103.648
Zr6	9655011	Zr1	4655011	40.403
Zr6	9655011	Zr1	4455011	140.253
Zr6	9455011	Zr5	8655021	97.462
Zr6	9455011	O1	11655011	159.855
Zr6	9455011	Zr5	8445011	76.352
Zr6	9455011	Zr1	4655011	139.597
Zr6	9455011	Zr1	4455011	39.747
Zr5	8655021	O1	11655011	67.799
Zr5	8655021	Zr5	8445011	39.817
Zr5	8655021	Zr1	4655011	120.288
Zr5	8655021	Zr1	4455011	134.022
O1	11655011	Zr5	8445011	83.666

	O1	11655011	Zr1	4655011	59.541
	O1	11655011	Zr1	4455011	157.976
	Zr5	8445011	Zr1	4655011	142.304
	Zr5	8445011	Zr1	4455011	114.955
	Zr1	4655011	Zr1	4455011	99.850
Zr7	Zr5	8555011	Zr5	8665021	104.913
	Zr5	8555011	O1	11655021	109.614
	Zr5	8555011	Zr7	10665021	55.771
	Zr5	8555011	Zr5	8455011	94.361
	Zr5	8555011	O1	11555021	160.855
	Zr5	8555011	Pb2	3555021	147.703
	Zr5	8555011	Zr5	8765021	62.070
	Zr5	8555011	Zr6	9655021	104.043
	Zr5	8555011	Zr6	9555021	148.067
	Zr5	8555011	Zr7	10655011	52.998
	Zr5	8555011	Zr7	10455011	127.002
	Zr5	8555011	Zr7	10565021	100.967
	Zr5	8555011	O1	11565011	58.883
	Zr5	8555011	Pb2	3655021	95.990
	Zr5	8555011	Pb2	3665011	30.770
	Zr5	8555011	Zr7	10765021	40.572
	Zr5	8555011	Zr5	8565021	124.439
	Zr5	8665021	O1	11655021	110.492
	Zr5	8665021	Zr7	10665021	49.141
	Zr5	8665021	Zr5	8455011	73.855
	Zr5	8665021	O1	11555021	79.722
	Zr5	8665021	Pb2	3555021	71.883
	Zr5	8665021	Zr5	8765021	76.174
	Zr5	8665021	Zr6	9655021	130.343
	Zr5	8665021	Zr6	9555021	105.652
	Zr5	8665021	Zr7	10655011	111.218
	Zr5	8665021	Zr7	10455011	68.782
	Zr5	8665021	Zr7	10565021	43.382
	Zr5	8665021	O1	11565011	54.561
	Zr5	8665021	Pb2	3655021	94.311
	Zr5	8665021	Pb2	3665011	81.917
	Zr5	8665021	Zr7	10765021	86.033
	Zr5	8665021	Zr5	8565021	44.360
	O1	11655021	Zr7	10665021	124.213
	O1	11655021	Zr5	8455011	152.787
	O1	11655021	O1	11555021	85.299
	O1	11655021	Pb2	3555021	47.587
	O1	11655021	Zr5	8765021	70.296
	O1	11655021	Zr6	9655021	20.438
	O1	11655021	Zr6	9555021	67.442
	O1	11655021	Zr7	10655011	57.948

O1	11655021	Zr7	10455011	122.052
O1	11655021	Zr7	10565021	145.159
O1	11655021	O1	11565011	149.976
O1	11655021	Pb2	3655021	25.818
O1	11655021	Pb2	3665011	138.224
O1	11655021	Zr7	10765021	83.745
O1	11655021	Zr5	8565021	123.593
Zr7	10665021	Zr5	8455011	79.723
Zr7	10665021	O1	11555021	125.925
Zr7	10665021	O1	11565011	25.764
Zr7	10665021	Pb2	3655021	98.395
Zr7	10665021	Pb2	3665011	37.551
Zr7	10665021	Zr7	10765021	49.178
Zr7	10665021	Zr5	8565021	80.264
Zr5	8455011	O1	11555021	68.757
Zr5	8455011	Pb2	3555021	114.496
Zr5	8455011	Zr5	8765021	134.898
Zr5	8455011	O1	11565011	54.873
Zr5	8455011	Pb2	3655021	165.981
Zr5	8455011	Pb2	3665011	68.299
Zr5	8455011	Zr7	10765021	123.445
Zr5	8455011	Zr5	8565021	40.985
O1	11555021	Pb2	3555021	51.439
O1	11555021	Zr5	8765021	136.442
O1	11555021	Zr6	9655021	85.702
O1	11555021	Zr6	9555021	27.646
O1	11555021	Zr7	10655011	143.247
O1	11555021	Zr7	10455011	36.753
O1	11555021	Zr7	10565021	69.312
O1	11555021	O1	11565011	113.458
O1	11555021	Pb2	3655021	102.231
O1	11555021	Pb2	3665011	136.453
O1	11555021	Zr7	10765021	157.716
O1	11555021	Zr5	8565021	47.152
Pb2	3555021	Zr5	8765021	86.493
Pb2	3555021	Zr6	9655021	62.154
Pb2	3555021	Zr6	9555021	54.110
Pb2	3555021	Zr7	10655011	97.190
Pb2	3555021	Zr7	10455011	82.810
Pb2	3555021	Zr7	10565021	97.604
Pb2	3555021	O1	11565011	126.430
Pb2	3555021	Pb2	3655021	53.297
Pb2	3555021	Pb2	3665011	150.850
Pb2	3555021	Zr7	10765021	107.794
Pb2	3555021	Zr5	8565021	76.598
Zr6	9655021	O1	11565011	160.489

	Zr6	9655021	Pb2	3655021	43.152
	Zr6	9655021	Pb2	3665011	134.783
	Zr6	9655021	Zr7	10765021	90.668
	Zr6	9655021	Zr5	8565021	131.397
	Zr6	9555021	Zr7	10655011	121.534
	Zr6	9555021	Zr7	10455011	58.466
	Zr6	9555021	Zr7	10565021	94.897
	Zr6	9555021	O1	11565011	138.006
	Zr6	9555021	Pb2	3655021	90.743
	Zr6	9555021	Pb2	3665011	149.735
	Zr6	9555021	Zr7	10765021	151.092
	Zr6	9555021	Zr5	8565021	74.181
	Zr7	10655011	Zr7	10455011	180.000
	Zr7	10655011	Zr7	10565021	142.486
	Zr7	10655011	O1	11565011	100.445
	Zr7	10655011	Pb2	3655021	43.894
	Zr7	10655011	Pb2	3665011	80.291
	Zr7	10655011	Zr7	10765021	31.535
	Zr7	10655011	Zr5	8565021	155.578
	Zr7	10455011	Zr7	10565021	37.514
	Zr7	10455011	O1	11565011	79.555
	Zr7	10455011	Pb2	3655021	136.106
	Zr7	10455011	Pb2	3665011	99.709
	Zr7	10455011	Zr7	10765021	148.465
	Zr7	10455011	Zr5	8565021	24.422
	Zr7	10565021	O1	11565011	44.147
	Zr7	10565021	Pb2	3655021	137.177
	Zr7	10565021	Pb2	3665011	70.207
	O1	11565011	Pb2	3655021	124.159
	O1	11565011	Pb2	3665011	29.346
	O1	11565011	Zr7	10765021	70.229
	O1	11565011	Zr5	8565021	66.850
	Pb2	3655021	Pb2	3665011	118.296
	Pb2	3655021	Zr7	10765021	61.627
	Pb2	3655021	Zr5	8565021	125.017
	Pb2	3665011	Zr7	10765021	56.669
	Pb2	3665011	Zr5	8565021	93.677
	Zr7	10765021	Zr5	8565021	127.486
O1	Zr6	9555011	Zr7	10655021	132.345
	Zr6	9555011	Pb2	3655011	119.386
	Zr6	9555011	Pb2	3555011	86.349
	Zr6	9555011	O1	11455011	68.850
	Zr6	9555011	O1	11655011	111.150
	Zr6	9555011	Zr7	10545011	149.434

	Zr7	10655021	Pb2	3655011	88.463
	Zr7	10655021	Pb2	3555011	133.619
	Zr7	10655021	Zr7	10555021	85.299
	Zr7	10655021	Zr5	8655021	33.089
	Zr7	10655021	Zr6	9655011	76.310
	Zr7	10655021	Zr5	8445011	72.977
	Zr7	10655021	Zr5	8545011	34.452
	Zr7	10655021	O1	11455011	122.052
	Zr7	10655021	O1	11655011	57.948
	Pb2	3655011	Pb2	3555011	92.282
	Pb2	3655011	Zr7	10555021	140.081
	Pb2	3655011	Zr5	8655021	117.592
	Pb2	3655011	Zr6	9655011	61.780
	Pb2	3655011	Zr5	8445011	102.753
	Pb2	3655011	Zr5	8545011	62.001
	Pb2	3655011	O1	11455011	131.939
	Pb2	3655011	O1	11655011	48.061
	Pb2	3655011	Zr7	10545011	89.435
	Zr5	8655021	O1	11455011	89.574
	Zr5	8655021	O1	11655011	90.426
	Zr6	9655011	O1	11455011	152.877
	Zr6	9655011	O1	11655011	27.123
	Zr 6	9655011	Zr7	10545011	103.154
	Zr5	8445011	O1	11455011	60.367
	O1	11455011	Zr7	10545011	100.445
	O1	11455011	Zr6	9455011	20.145
	O1	11455011	Zr1	4555011	81.935
	O1	11455011	Zr4	7655011	97.043
	O1	11655011	Zr7	10545011	79.555
	O1	11655011	Zr6	9455011	159.855
	O1	11655011	Zr1	4555011	98.065
	O1	11655011	Zr4	7655011	82.957
U1	U1	7555011	Zr3	6555011	121.543
	U1	7555011	Zr3	6655011	110.905
	Zr4	7555011	O2	12655011	84.956
	U1	7555011	O2	12455011	95.044
	U1	7555011	U4	7455011	54.573
	Zr4	7555011	Zr2	5555011	36.451
	Zr4	7555011	Zr4	7655011	48.398
	Zr3	6555011	Zr3	6655011	67.449
	U1	6555011	O2	12655011	117.116

SEM(SCANNING ELECTRON MICROSCOPY)

Scanning electron microscopy (SEM) is giving morphological examination with direct visualization. The techniques based on electron microscopy offer several advantages in morphological and sizing analysis; however, they provide limited information about the size distribution. For SEM characterization, nanoparticles solution should be first converted into a dry powder, which is then mounted on a sample holder followed by coating with a conductive metal, such as gold, using a sputter coater. The sample is then scanned with a focused fine beam of electrons. The surface characteristics of the sample are obtained from the secondary electrons emitted[12] from the sample surface. The morphology of the oxide nanoparticles is shown in Fig.2. From the image, it is clear that the particles were highly agglomerated in nature. The SEM pictures clearly show randomly distributed grains with smaller size. From the SEM analyses, one can conclude the formation of nanoparticles spherical structure. Here it is grown in very high-density and possessing almost uniform spherical shapes. The image reveals that the average size of the particles is 18.32 nm.

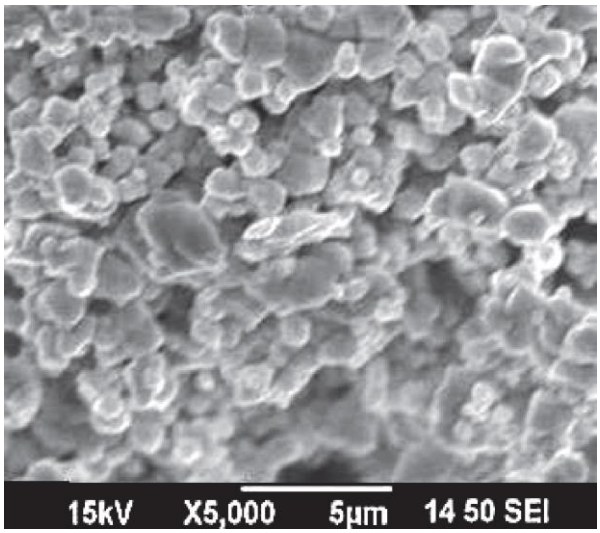

Figure .4 SEM image of **$Pb_{0.5}U_{0.25}Zr_{1.25}O_{4.5}$**

THE TRANSMISSION ELECTRON MICROSCOPE (TEM)

The transmission electron microscope utilized a high energy electron beam transmitted through a very thin sample to image and analyzes the microstructure of materials with atomic scale resolution. The electrons are focused with electromagnetic lenses and the image is observed on a fluorescent screen, or recorded on film or digital camera. The electrons are accelerated at several hundred kV, giving wavelengths much smaller than that of light: 200kV electrons have a wavelength of 0.025Å. Whereas, the resolution of the optical microscope is limited by the wavelength of light, that of the electron microscope is limited by aberrations inherent in electromagnetic lenses, to about 1–2 Å. Transmission electron microscope is used to characterize

the microstructure of materials with very high spatial resolution. The transmission electron microscopic study was carried out to confirm the actual size of the particles, their growth pattern and the distribution of the crystallites[13]. TEM image of the synthesized silver oxide nanoparticles is shown in Fig.3. As can be seen from the TEM image, the particles are nearly spherical shapes with well defined boundaries. It is evident from the micrographs that the average size of the particles as directly measured from the image is 18.32 nm. This result is similar to that obtained from XRD analysis.

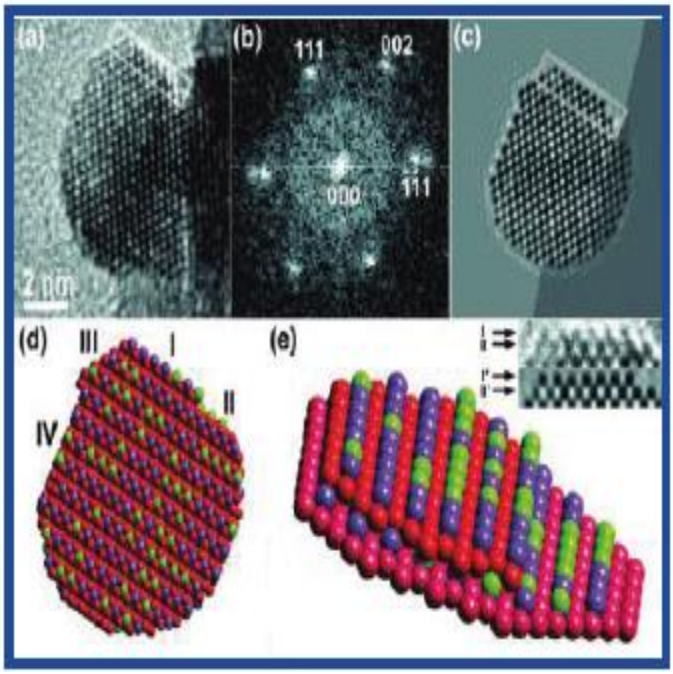

Figure 5. High-resolution TEM image of a faceted crystallite of **Pb** $_{0.5}$ **U**$_{0.25}$ **Zr** $_{1.25}$ **O**$_{4.5}$ with one facet highlighted

TEM analysis confirms the presence of small crystallites making up our samples, and Figure 2 shows some representative images that show the maximum particle dimension is around 10 nm. These images apparently show a dependence of particle size on composition, with the most Bi-rich materials showing smaller crystallites on average. The bulk, average particle size will be explored in more detail below when we discuss the neutron scattering results. Higher resolution TEM, Figure 3, reveals that the small crystallites show faceted surfaces: this illustrates the high crystallinity of individual particles[14].

DIELECTRIC CONSTANT

The dielectric constant and the dielectric loss of the 10 mm in diameter pellet have been used for the determination of dielectric properties of silver oxide nanoparticles. The corresponding thickness of the pellet was 1.20 mm was studied at different temperature using a HIOKI 3532-50 LCR HITESTER in the frequency range of 50 Hz to 5 MHz. The results of the dielectric constant and dielectric loss as a function of frequency have been plotted in Figs. 6&7. It can be easily interpreted from the plots that the silver oxide nanoparticles show same trend, as having high values of dielectric constant and dielectric loss at low frequencies and decrease with the increase

in frequency while reaching to a constant saturated value at high frequencies, depicting a frequency independent behavior. These defects activate interfacial polarizations at low frequencies. Due to this polarization, the dielectric constant is higher at low frequencies. The net polarization of silver oxide is owing to ionic, electronic, dipolar and space charge polarizations [10]. The huge value of the dielectric constant is due to the fact that silver oxide acts as a nanodipole under electric fields [15]. The small-sized particles require a large number of particles per unit volume, important in an increase of the dipole moment per unit volume, and a high dielectric constant. The dielectric constant at low frequencies starts from high value and decreases with increase in temperature. As the temperature increases, the dielectric constant values start increasing. The high value of dielectric constant at low temperature credited to space charge polarization whereas at higher temperature and at low frequencies it possibly connected with defect related conduction processes [16]. The variations of dielectric loss of silver oxide nanoparticles of with frequency and temperature are shown in Fig.7. It can be seen that dielectric loss decreases with increase of frequency and at higher frequencies the loss angle has almost the same value at all temperatures. In dielectric materials, generally dielectric losses take place due to absorption current. The orientation of molecules along the direction of the applied electric field in polar dielectrics requires a part of electric energy to overcome the forces of internal friction [13]. One more part of electric energy is utilized for rotations of dipolar molecules and other kinds of molecular transfer from one position to another, which also involve energy losses. In nanophase materials, inhomogeneities similar to defects and space charge formation in the inter phase layers create an absorption current ensuing in a dielectric loss [17].

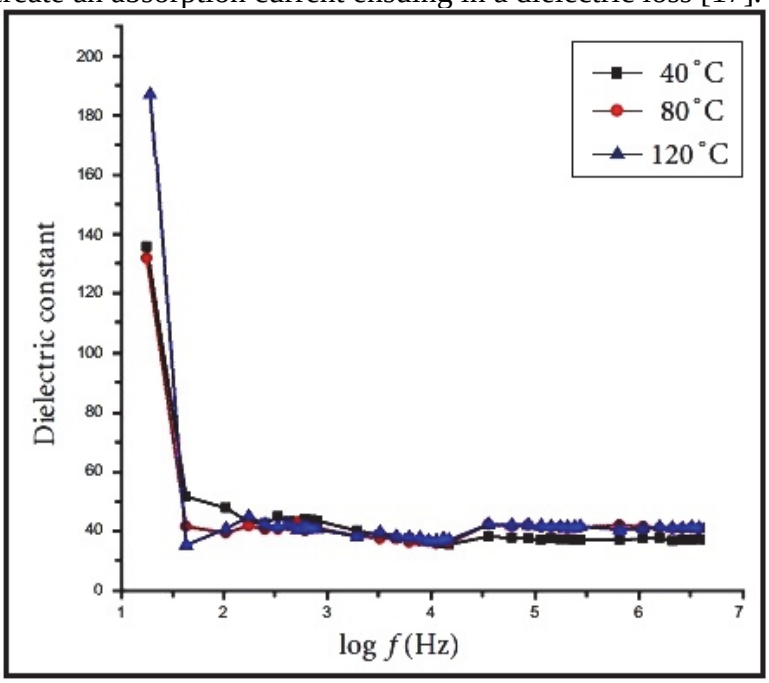

Figure 6..: Dielectric constant as a function of log frequency

The titled metal oxide show nanopartice according to particle size which are placed in the heater and their response is taken at different temperatures. Temperature dependent dielectric constant and dielectric loss has been plotted in Figs. 8 and 9. It is also observed that as the temperature increases, the dielectric constant also increases to a considerable value as seen in Fig. 5. The same trend is observed behavior of dielectric properties with temperature is different over

different temperature ranges i.e. at low and high temperature. It is evident from the Fig.6 and 7 that the dielectric constant and dielectric loss are low at a certain room temperature range and remain independent of temperature changes. In high temperature range the dielectric properties rise suddenly and reach a maximum value. The basic reason of the independency of dielectric constant in low temperature range is that impurities remain localized in this range and so conduction is not easy while at high temperature impurities are no more localized and hence conductivity of the material is increased. In case of ionic solids, electrons of the material also become free and contribute to conduction. This results in high polarization of the material; hence value of dielectric constant is increased with increase in temperature. At low and room temperature range, the effect of grain boundaries is dominant and that is why the dielectric properties have small magnitudes and are constant. As the temperature is increased, the role of grains becomes more and more effective and increases in the dielectric properties

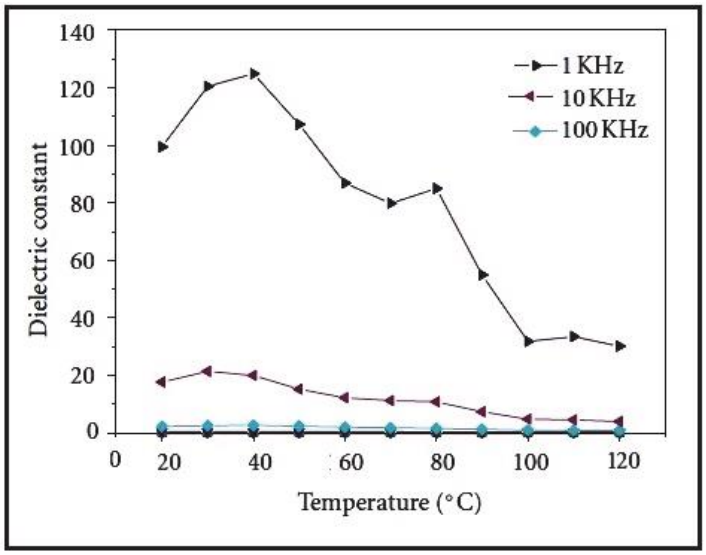

Figure. 7: Temperature dependent dielectric constant of **$Pb_{0.5}U_{0.25}Zr_{1.25}O_{4.5}$**

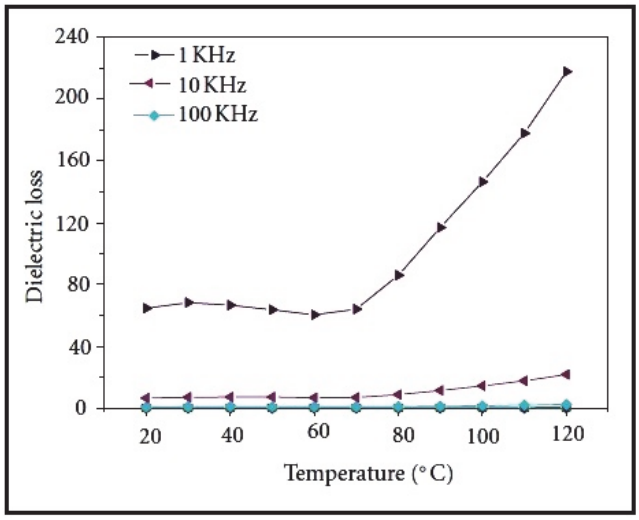

Figure 8. Dielectric loss versus temperature

Due to the thermionic emission and tunnelling of charge carriers across the barrier, the conductivity increases with the temperature. Because of small size of the particles, the charge carriers reach the surface of the particles more and easily enabling the electron transfer by thermionic emission or tunneling to enhance the conductivity [17]. The a.c. conductivities strongly depend on the particle size, the concentration and heat treatment ofthe sample and the permeating of the electrolytes. Also, the frequency dependent data indicated that the

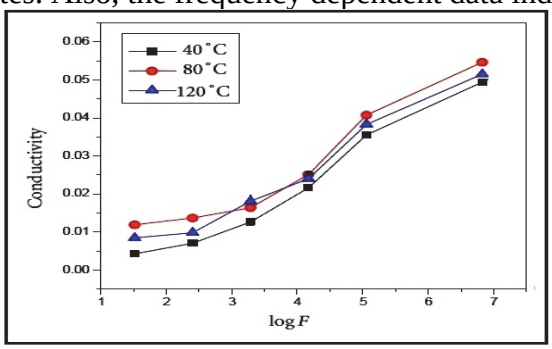

Fig.9 Variation of conductivity with log f

enhancement was due to grains rather than grain boundary or surface conduction. The nature of frequency and temperature dependence of a.c. conductivity of the present samples, suggests an electronic hopping mechanism, exhibited by a large number of nanocrystalline materials. This hopping mechanism is compatible with the highly order and crystal structure of the grain boundary layers of nanophase materials, having high densities of localized levels. This polarization, which is out of phase with the applied electric field, is measured as a.c. conductivity.

CONCLUSIONS

The titled mixed valence nanoparticles have been successfully synthesized using stoichiometry chemical technique. X-ray diffraction analysis reveals that the crystallite size of the oxide \particles was found to be 18.32 nm. Spherical shapes morphology of the prepared mixed valence metal oxide was observed in the SEM studies. The transmission electron microscopic analysis confirms the prepared **Pb $_{0.5}$ U$_{0.25}$ Zr $_{1.25}$ O$_{4.5}$** with the particle size of around18.32 nm. Absorption spectrum revealed that the extended absorption wavelength towards the visible-light region. The value of band gap energy obtained from UV absorption spectrum is 570 eV, which was also attributed to the formation of nanocrystalline particles. The variation of dielectric constant, dielectric loss with frequency and temperature for **Pb $_{0.5}$ U$_{0.25}$ Zr $_{1.25}$ O$_{4.5}$** nanoparticles were analyzed. In addition, the plasma energy of the valence electron, Penn gap or average energy gap, the Fermi energy and electronic polarizability of the **Pb $_{0.5}$ U$_{0.25}$ Zr $_{1.25}$ O$_{4.5}$** nanoparticles have been also determined. AC electrical conductivity was found to increase with an increase in the temperatures and frequency. The structure was demined by powder XRD using Rietveld refinement. This oxide will be shown as semi- conductivity character. The ac conductivity plot of the pelletized form of $Bi_{0.5}Mn_{0.64}Mo_{1.5}O_{0.41}$ nanoparticles is shown in Fig6 .It is observed from the results that the ac conductivity increases with the increase in temperature, which shows the semiconducting nature of the **Pb $_{0.5}$ U$_{0.25}$ Zr $_{1.25}$ O$_{4.5}$**

REFERENCES

1.Parveen Rathi , Dharam Pal Singh , Parveen Surain , Synthesis, characterization, powder XRD and antimicrobial-antioxidant activity evaluation of trivalent transition metal macrocyclic complexes, C. R. Chimie 18 (2015) 430–437
2.KaiLiandRikVanDeun,NovelIntenseEmissionTunableLi1.5La1.5WO6:Mn4+,Nd3+,Yb3+Material with Good Luminescence Thermal Stabilit forPotential Applications in c‑Si Solar Cells and Plant-Cultivation Far-Red-NIR LEDs, ACS Sustainable Chem. Eng. 2019, 7, 16284−16294
3.Peng, Q.; Cao, R.; Ye, Y.; Guo, S.; Hu, Z.; Chen, T.; Zheng, G. Photoluminescence properties of broadband deep-red-emitting Na2MgAl10O17:Mn4+ phosphor. J. Alloys Compd. 2017, 725, 139−144.
4. Liu, Y.; Gao, G.; Huang, L.; Zhu, Y.; Zhang, X.; Yu, J.; Richards, B. S.; Xuan, T.; Wang, Z.; Wang, J. Co-precipitation synthesis and photoluminescence properties of BaTiF6:Mn4+: an efficient red phosphor for warm white LEDs. J. Mater. Chem. C 2018, 6, 127−133.
5. Yu, Y.; Huang, Y.; Zhang, L.; Lin, Z.; Wang, G. Assessment of structure and spectral characteristics of new laser crystal Nd3+:KBaY- (MoO4)3. J. Alloys Compd. 2015, 651, 164−169.
6. Marciniak, Ł.; Bednarkiewicz, A.; Hreniak, D.; Strek, W. The influence of Nd3+ concentration and alkali ions on the sensitivity of non-contact temperature measurements in ALaP4O12:Nd3+ (A = Li, K, Na, Rb)nanocrystalline luminescent thermometers. J. Mater. Chem. C 2016, 4, 11284−11290.
7. Yang, Z.; Yang, J.; Qiu, J.; Song, Z. Comprehensive investigations of near infrared downshift and upconversion luminescence mechanisms in Yb3+ single-doped and Er3+,Yb3+ codoped SiO2 inverse opals. Phys. Chem. Chem. Phys. 2017, 19, 31997−32006.
8. Ye, S.; Zhou, J.; Wang, S.; Hu, R.; Wang, D.; Qiu, J. Broadband downshifting luminescence in Cr3+-Yb3+ codoped garnet for efficient photovoltaic generation. Opt. Express 2013, 21, 4167.
9. Reisfeld, R.; Lieblich-Soffer, N. Energy transfer from UO_2^{2+} to Sm^{3+} in phosphate glass. J. Solid State Chem. 1979, 28, 391−395.
10. Dexter, D. L.; Schulman, J. H. Theory of Concentration Quenching in Inorganic Phosphors. J. Chem. Phys. 1954, 22, 1063−1070.
(49) Blasse, G.; Grabmaier, B. C. Luminescent Materials; Springer-Verlag: Berlin, Germany, 1994.
11. Wu, L.; Bai, Y.; Wu, L.; Yi, H.; Zhang, X.; Zhang, L.; Kong, Y.; Zhang, Y.; Xu, J. Analysis of the structure and abnormal photoluminescence of a red-emitting LiMgBO3:Mn2+ phosphor. Dalton Trans. 2018, 47, 13094−13105.
12. *Parashuram Mishra* Synthesis, crystal structure determination and ionic properties of novel BiCa0.5Mg0.5 O2.5 via X- ray powder diffraction data , Elixir Crystal Growth. 2041 32 (2011) 2041-2045.
13. T. Dan Vu, Firas Krichen, Maud Barre,† Sandrine Coste,† Alain Jouanneaux, Emmanuelle Suard,Andrew Fitch, and François Goutenoire Ab Initio Structure Determination of La34Mo8O75 Using Powder X-ray and Neutron Diffraction Data, DOI: 10.1021/acs.cgd.8b01552 Cryst. Growth Des. XXXX, XXX, XXX−XXX
14. Chambrier, M.-H.; Le Bail, A.; Giovannelli, F.; Redjaimia, A.;Florian, P.; Massiot, D.; Suard, E.; Goutenoire, F. La10W2O21: AnAnion-Deficient Fluorite-Related Superstructure with Oxide Ion Conduction. Inorg. Chem. 2014, 53, 147−159.

15. Lopez-Vergara, A.; Porras-Vazquez, J. M.; Infantes-Molina, A.; Canales -Vazquez, J.; Cabeza, A.; Losilla, E. R.; Marero-Lopez, D.Effect of Preparation Conditions on the Polymorphism and Transport Properties of La6−xMoO12−δ (0 ≤ x ≤ 0.8). Chem. Mater. 2017, 29,6966−6975.

16. Dmitri O. Charkin , Andrey S. Karpov , Sergey M. Kazakov , Igor V. Plokhikh ,Anastasiya I. Zadoya c, Alexey N. Kuznetsov a, Konstantin I. Maslakov a, Anton Yu Teterin d,Yury A. Teterin , Alexander N. Zaloga e, Oleg I. Siidra c, f Synthesis, crystal structure, spectroscopic properties, and thermal behavior of rare-earth oxide selenates, Ln2O2SeO4 (Ln ¼ La, Pr, Nd): The new perspectives of solid-state double-exchange synthesis, Journal of Solid State Chemistry 277 (2019) 163–168

17. Owen P. Missen[1,2]* , Anthony R. Kampf[3], Stuart J. Mills[1], Robert M. Housley[4], John Spratt[5], Mark D. Welch[6],Mark F. Coolbaugh[7], Joe Marty[8], Marek Chorazewicz[9] and Cristiano Ferraris[10]
The crystal structures of the mixed-valence tellurium oxysalts tlapallite, (Ca,Pb)3CaCu6[Te4+ 3 Te6+O12]2(Te4+O3)2(SO4)2·3H2O, and carlfriesite, CaTe4+2 Te6+O8, Mineralogical Magazine (2019), 83, 539–549doi:10.1180/mgm.2019.9

View publication stats